Polyhedron 118 (2016) 159–170

Contents lists available at ScienceDirect

Polyhedron

journal homepage: www.elsevier.com/locate/poly

Design and synthesis of non-symmetric phenylpyridine type ligands. Experimental and theoretical studies of their corresponding iridium complexes

C. Iturbe [a], B. Loeb [a,*], M. Barrera [a], I. Brito [b], A. Cañete [a,*]

[a] Facultad de Química, Pontificia Universidad Católica de Chile, Vicuña Mackenna 4860, Santiago, Chile
[b] Departamento de Química, Universidad de Antofagasta, Avda. Angamos 601, Antofagasta, Chile

ARTICLE INFO

Article history:
Received 12 June 2016
Accepted 22 July 2016
Available online 5 August 2016

Keywords:
Non-symmetric phenylpyridine ligands
Iridium complexes
Molecular calculations
NMR spectroscopy
Electrochemical studies

ABSTRACT

In this work three non-symmetric phenylpyridine type ligands, **L1**, **L2** and **L3**, were designed, and their corresponding Iridium complexes, **C1**, **C2** and **C3**, synthetized, in order to understand the effect of ligand asymmetry on the properties of the complexes, and to explore their potentiality in devices. The complexes were structurally characterized by NMR experiments and by X-ray Diffraction, and physicochemically by technics as UV/Vis and cyclic voltammetry. Theoretical DFT calculations of the energy and electronic density of the frontier orbitals of the complexes under study were also performed. The energy of the HOMO and LUMO correlated well with the experimental electrochemical data, and supported the understanding of the processes observed.

1. Introduction

Transition Metal Chromophores have attracted great attention for their capacity to respond in different applications. In this ambit, polypiridyl compounds of transition metals, as $Ru(bpy)_3^{2+}$, or cyclometallated complexes, as $Ir(ppy)_2(acac)$, are good triplet emitters and have suitable spectral properties for different applications, *e.g.*, in OLEDs devices, or as dyes fixed to TiO_2 in solar cells, among others [1,2]. For this kind of complexes, the ligand plays an important role to induce different photophysical properties or electrochemical behaviors [3]. Accordingly, in the literature there are many spectral studies with ligands based on 2-phenylpyridine (ppy) or 2,2′-bipyridine (bpy), coordinated to different transition metals [4]. Complexes with red-orange to deep red phosphorescence and high emission quantum yields have been obtained. This kind of properties are related to the gap between the lowest unoccupied molecular orbital (LUMO) to the highest occupied molecular orbital (HOMO). In special, it is possible to adjust the HOMO–LUMO gap simply by changing the ligand framework; this change affects directly the emission color [5–7]. For example, given its donor properties, in complexes with ligands of 2-phenylpyridine (ppy) type, the HOMO energy level is destabilized compared to the equivalent complexes with bpy type ligands. This reduces the HOMO–LUMO energy gap, and shifts the absorption and emission maxima to the red. Additionally, in complexes with ppy type ligands the HOMO electronic density is localized both over the phenyl ring and the metal center, while the LUMO level is centered in the pyridine ring [8]. In literature, the reported synthetic procedures on substituted bpy or ppy type ligands has been mainly been focused on symmetrically substituted ligands.

The present study is oriented to the understanding of the effect of the symmetry of the ligand, and its substituents, on some of the properties of the corresponding complexes. The ligands used are non-symmetric derivatives of ppy, and are tested on Iridium complexes of type $Ir(R\text{-}ppy)_2(acac)$. The ligands and complexes were spectroscopically and crystallographically characterized. A theoretical study was also performed, in order to understand the tendencies observed in the experimental results for the series of Iridium complexes with non-symmetric ppy ligands studied.

2. Experimental

2.1. General methods

All starting materials were commercially available and used as received without further purification. Thin Layer Chromatography (TLC) was performed on silica gel 60 F_{254}, using aluminum plates and visualized with vanillin stain and UV lamp. Flash chromatography was carried out on hand packed columns of silica gel 60 (230–400 mesh). All NMR experiments were recorded on a Bruker

* Corresponding authors.

http://dx.doi.org/10.1016/j.poly.2016.07.029
0277-5387/

Avance of 400 MHz, ^{1}H NMR spectra were recorded at 400 MHz using $CDCl_3$ as the solvent and TMS as internal standard (0.00 ppm). ^{13}C NMR spectra were recorded in $CDCl_3$ at 101 MHz. The electrochemical characterization of the Iridium complex was performed by means of cyclic voltammetry (CV) in ACN as a solvent, using a three-electrode cell consisting of a platinum working electrode, a platinum wire auxiliary electrode and standard Ag/AgCl electrode as the reference electrode with a scan rate of 100 mV * s^{-1}. The solutions were 1×10^{-1} mol/L^{-1} in the corresponding complex, and contained tetrabutylamonium hexafluorophosphate 1×10^{-1} mol/L^{-1} as supporting electrolyte. The emission spectra were recorder on a PerkinElmer LS 55 Fluorescence spectrometer with slit of 2.5 cm. The absorption spectra were recorder on a Shimadzu UV-3101PC UV–VIS-NIR Spectrophotometer. The X-rays diffraction were obtained on a STOE IPDS II two-circle. The structure was solved by direct methods using SHELXS; and Figures were created using the PLATON software. Finally, for the quantum yields for all complexes, using [Ru $(bpy)_3](PF_6)_2$ as reference compound was calculated using standard reported methods [9].

3. Computational details

All calculations were performed on ADF framework [10] and the geometries were optimized with the OPBE [11] exchange correlation functional, including the scalar relativistic correction [12] in conjunction with ZORA-TZP and DZP basis set for Iridium and atoms from the first row. Hirschfeld fragment analysis [13] was employed to study the composition of the molecular orbitals in sets of four fragments, including the metal core(M), the ancillary acac ligand(L), and the phenylpyridine ligand, which in turn is decomposed in the two fragments: phenyl(F) and piridyne(P). The TDDFT calculations were performed in presence of acetonitrile as solvent and employing a Klamt surface [14]. The first 40 allowed and not allowed excitations were calculated with ZORA-SZ basis set for C,H,N,O and the SOAP exchange correlation potential [15].

3.1. Procedure for ligand synthesis

3.1.1. Preparation of methyl 2-(m-tolyl)isonicotinate (**L1**) [16]

*3.1.1.1. 2-Bromoisonicotinic acid (**2**).* A mixture of 2-bromo-4-methylpiridine, 1, (9.27 g, 54 mmol) in 490 mL of water, and of $KMnO_4$ (16 g, 11 mmol) in 250 mL of water were stirred for 5 h at 110 °C. The resulting mixture was filtered and the filtrate was reduced to 1/3 and acidified with HCl until pH 3. The white precipitated obtained was filtered and dried, Yield: 36% of 2-bromoisonicotinic acid.

FT-IR (KBr) ν, 3100–2350 (stretching O–H), 1710 (str. C=O), 1597 (str. C=C), 1546 (str. C=N), 1285 (str. C–O), 667 (str. C-Br) cm^{-1}. ^{1}H NMR (400 MHz, DMSO-d_6, ppm) δ, 8.58 (dd, J = 5.0, 0.8 Hz), 7.95 (dd, J = 1.4, 0.8 Hz), 7.84 (dd, J = 5.0, 1.4 Hz).

*3.1.1.2. Methyl 2-bromoisonicotinate (**3**).* A mixture of 2-bromoisonicotinic acid, **2**, (0.200 g, 0.99 mmol) in acetone and K_3PO_4 (0.290 g, 1.09 mmol) was stirred for 30 min at room temperature. When the time was over CH_3I (0,155 g, 1.09 mmol) was added and the mixture refluxed for 2 h. Finally the mixture was cooled and left over ice, and the product extracted with $CHCl_3$. The organic phase was dried with Na_2SO_4, and purified by silica gel chromatography with $CHCl_3$ as mobile phase. The contents of the organic phase were removed *in vacuo* to obtain methyl 2-bromoisonicotinate with 82% yield.

FT-IR (KBr) ν = 3089 (str. C–H sp_3), 2955 (str. C–H sp2), 1722 (str. C=O), 1588 (str. C=C aromatic), 1546 (str. C=N), 670 (str. C-Br) cm^{-1}. ^{1}H NMR (400 MHz, $CDCl_3$, ppm) δ 8.36 (d, J = 5.1 Hz, 1H), 7.85 (s, 1H), 7.65 (d, J = 5.0 Hz, 1H), 3.82 (s, 3H).

*3.1.1.3. Methyl 2-(m-tolyl)isonicotinate (**L1**).* In a micro reactor vessel, bromopyridne (**3**) (3.1 eq), 30 mL of DME, and $Pd(Ph_3)_4$ (0.015 eq) were added. The mixture was stirred for 10 min under inert atmosphere. When the time was over, boronic acid (**4,** 1.2 eq) and K_2CO_3 (2.4 eq) were added. The mixture was heated at its boiling point for 2 days. Finally the reaction was filtered under vacuum and the filtrate was extracted with $CHCl_3$. The crude product was purified by silica gel chromatography using petroleum benzine/ethyl acetate (1:1) as mobile phase. The contents of the organic phase were removed *in vacuo* to obtain an orange oil corresponding to methyl 2-(*m*-tolyl)isonicotinate, **L1**, with 80% yield.

^{1}H NMR (400 MHz, $CDCl_3$, ppm) δ, 8.81 (d, J = 5.0 Hz, 1H), 8.28 (s, 1H), 7.88 (s, 1H), 7.82 (d, J = 7.8 Hz, 1H), 7.75 (dd, J = 5.0, 1.3 Hz, 1H), 7.37 (t, J = 7.7 Hz, 1H), 7.27 – 7.23 (m, 1H), 3.97 (s, 3H), 2.44 (s, 3H). ^{13}C NMR (101 MHz, $CDCl_3$, ppm) 165.79, 158.62, 150.31, 138.57, 138.37, 138.14, 130.36, 128.79, 127.78, 127.64, 124.19, 121.05, 119.96, 119.77, 77.16, 52.75, 21.52.

*3.1.1.4. Methyl 2-phenylisonicotinate (**L2**).* This ligand was obtained with 86% yield using a similar procedure than the one described for **L1**.

^{1}H NMR (400 MHz, CDCl3, ppm) δ, 8.75 (d, J = 4.8 Hz, 1H), 8.21 (s, 1H), 7.97 (d, J = 7.2 Hz, 2H), 7.68 (d, J = 4.8 Hz, 1H), 7.39 (dt, J = 21.7, 7.0 Hz, 3H), 3.90 (s, 3H). ^{13}C NMR (101 MHz, $CDCl_3$, ppm), 165.88, 158.57, 150.55, 138.61, 138.2, 129.58, 128.97, 127.10, 121.23, 119.81, 52.83.

*3.1.1.5. Methyl 2-(m-tolyl)pyridine (**L3**).* This ligand was obtained with 86% yield using a similar procedure than the one described for **L1**.

^{1}H NMR (400 MHz, $CDCl_3$, ppm) δ 8.53 (d, J = 4.9 Hz, 1H), 7.97 (d, J = 7.2 Hz, 2H), 7.52 (s, 1H), 7.45 (t, J = 7.3 Hz, 2H), 7.39 (d, J = 7.2 Hz, 1H), 7.02 (d, J = 4.4 Hz, 1H), 2.38 (s, 3H). ^{13}C NMR (101 MHz, $CDCl_3$, ppm) δ 157.45, 149.50, 147.79, 139.62, 128.81, 128.70, 127.01, 123.20, 121.60, 21.28.

3.2. General procedure to obtain [Ir(C^N)2(μ-Cl)]$_2$ dimers [17]

All dimers were synthetized by the following procedure:

To a 100 mL round bottom flask 1 eq of $IrCl_3$ in methylethylene glycol (5 mL for each 150 mg) were added. The flask was attached to a condenser and the system set under nitrogen atmosphere, and then the corresponding L(*i*) ligand (2.5 eq) was added. The reaction was carried out at reflux in a silicone bath for a period of 12 h. Then, the heating was stopped and the reaction allowed to cool. The contents of the flask were removed in *vacuo* to afford the crude compound was purified with a minimal amount of hexane/ethyl acetate (1:1) and stirred a few seconds. Finally, a few drops of hexane were added to precipitate the complex that was separated from the solution by filtering, yield 98%.

*3.2.1. Bis[μ-chloro di-(2-m-tolylisonicotinate)iridium III] (**5**),*

^{1}H NMR (400 MHz, $CDCl_3$, ppm) δ 9.31 (d, J = 6.0 Hz, 3H), 8.42 (s, 3H), 7.44 (s, 3H), 7.39–7.08 (m, 5H), 6.45 (d, J = 7.5 Hz, 3H), 5.77 (d, J = 7.9 Hz, 3H), 4.12 (s, 9H), 2.15 (s, 10H). ^{13}C NMR (101 MHz, $CDCl_3$, ppm) δ 169.30, 164.80, 151.54, 142.26, 140.85, 137.12, 130.87 (d), 129.99, 125.00, 120.80, 117.69, 52.89, 20.65.

*3.2.2. Bis[μ-chloro di(2-phenylisonicotinate)iridium III] (**6**)*

Yield 99%. ^{1}H NMR (400 MHz, $CDCl_3$, ppm) δ 9.32 (s, 1H), 8.45 (s, 1H), 7.63 (d, J = 7.6 Hz, 1H), 7.20 (d, J = 5.5 Hz, 1H), 6.81 (t, J = 7.3 Hz, 1H), 6.61 (t, J = 7.4 Hz, 1H), 5.90 (d, J = 7.7 Hz, 1H), 4.12 (s, 3H). ^{13}C NMR (101 MHz, $CDCl_3$, ppm) δ 169.64, 164.96,

151.89, 145.32, 142.80, 137.73, 130.63, 130.02, 124.66, 122.14, 121.35, 118.15, 53.23.

*3.2.3. Bis[μ-chloro di-2-(m-tolyl)pyridinyl)iridium III] (**7**)*

Yield > 99%. ^{1}H NMR (400 MHz, $CDCl_3$, ppm) δ 9.24 (d, *J* = 4.5 Hz, 1H), 7.82 (d, *J* = 7.4 Hz, 1H), 7.66 (t, *J* = 6.9 Hz, 1H), 7.29 (s, 1H), 6.76–6.66 (m, 1H), 6.40 (d, *J* = 7.2 Hz, 1H), 5.80 (d, *J* = 7.6 Hz, 1H), 2.10 (s, 3H). ^{13}C NMR (101 MHz, $CDCl_3$, ppm) δ 152.14, 143.95, 136.26, 130.74, 130.43, 124.77, 122.19, 118.58, 77.70, 77.38, 77.06, 21.21.

3.3. General procedure to obtain [Ir(C^N)$_2$(acac)] [17]

To a 100 mL round bottom flask 1 eq of *[Ir(C^N)$_2$ (μ-Cl)]$_2$* and 2 eq of acac in presence of TBAOH were added, using CH_2Cl_2 as solvent. This reaction was refluxed for a period of 12 h. Then, the heating was stopped and the reaction allowed to cool. The contents of the flask were removed *in vacuo* to afford the crude compound, which was purified by successive washes with hexane. The precipitated complex was separated from the solution by filtration.

*3.3.1. Acetylacetonate-di-2-(m-tolyl)isonicotinate iridium III, **C1***

^{1}H NMR (400 MHz, $CDCl_3$, ppm) δ 8.63 (d, *J* = 5.9 Hz, 2H), 8.38 (s, 2H), 7.63 (dd, *J* = 5.9, 1.6 Hz, 2H), 7.48 (s, 2H), 6.57 (d, *J* = 8.6 Hz, 2H), 6.10 (d, *J* = 7.7 Hz, 2H), 5.20 (s, 1H), 4.04 (s, 5H), 2.20 (s, 6H), 1.78 (s, 6H). ^{13}C NMR (101 MHz, $CDCl_3$, ppm) δ 184.77, 169.40, 165.01, 148.28, 144.24, 143.70, 143.26 (d), 137.50, 132.41, 130.95, 129.99, 125.12, 120.63, 117.66, 100.34, 52.75, 28.55, 20.85.

*3.3.2. Acetylacetonate-di-2-phenylisonicotinate iridium III, **C2***

^{1}H NMR (400 MHz, $CDCl_3$, ppm) δ 8.65 (d, *J* = 5.9 Hz, 2H), 8.42 (s, 2H), 7.66 (d, *J* = 6.5 Hz, 4H), 6.85 (t, *J* = 7.4 Hz, 2H), 6.71 (t, *J* = 7.3 Hz, 2H), 6.22 (d, *J* = 7.5 Hz, 2H), 5.22 (s, 1H), 4.04 (s, 6H), 1.79 (s, 6H). ^{13}C NMR (101 MHz, $CDCl_3$, ppm) δ 185.23, 169.77, 165.24, 148.66, 147.81, 143.86, 138.07, 133.09, 129.87, 124.69, 121.22, 120.07, 118.13, 100.68, 53.07, 28.83.

*3.3.3. Acetylacetonate-di-2-(m-tolyl)pyridine iridium III, **C3***

^{1}H NMR (400 MHz, $CDCl_3$, ppm) δ 8.50 (d, *J* = 5.4 Hz, 2H), 7.82 (d, *J* = 7.9 Hz, 2H), 7.69 (t, *J* = 7.7 Hz, 2H), 7.37 (s, 2H), 7.10 (t, *J* = 6.1 Hz, 2H), 6.54 (d, *J* = 7.1 Hz, 2H), 6.15 (d, *J* = 7.7 Hz, 2H), 5.20 (s, 1H), 2.18 (s, 3H), 1.77 (s, 3H). ^{13}C NMR (101 MHz, $CDCl_3$, ppm) δ 184.62, 168.79, 148.31, 144.77, 143.35, 136.73, 132.87, 130.62, 129.61, 124.76, 121.37, 118.36, 100.44, 28.88, 21.21.

4. Results and discussion

4.1. Synthesis and characterization

In the present work three non-symmetric phenylpyridine-based ligands were synthetized: 2-(*m*-tolyl)isonicotinate, (**L1**), 2-phenylisonicotinate, (**L2**), *m*-tolyl)pyridine, (**L3**), and used as starting materials to synthetize Iridium (III) cyclometalated complexes, in order to evaluate the effect of ligand asymmetry on the complex properties, and eventually to predict their potentiality in solar cells and OLED devices. Ligands were synthetized using 2-bromo-4-methylpyridine **1** as starting material; the methyl group of **1** was oxidized by conventional methodology using $KMnO_4$ to prepare the respective acid **2**. Subsequently, this acid was sterificated by methyl iodide in basic media to obtain **3**. By a Suzuki–Miyaura reaction between **3** and **4** it was possible to obtain the **L1** ligand (Scheme 1).

By the same strategy, the ester **3**, or 2-bromopyridine, and the respective boronic acid under Suzuki–Miyaura conditions allowed to obtain the C^N ligands **L2** and **L3** (Scheme 2).

To obtain the Ir(C^N)$_2$(acac) complexes it is necessary to first prepare the corresponding dimer intermediates [Ir(C^N)$_2$(μ-Cl)]$_2$; in this case, these intermediates were synthesized by the reaction between $IrCl_3$ and the respective C^N ligand to obtain the following complexes: *[Ir(L1)$_2$ (μ-Cl)]$_2$*, (**5**), *[Ir(L2)$_2$ (μ-Cl)]$_2$*, (**6**) and *[Ir(L3)$_2$ (μ-Cl)]$_2$*, (**7**) [18–20].

Subsequently, the *Ir(C^N)$_2$(acac)* compounds, *Ir(L1)$_2$(acac)* **C1**, *Ir(L2)$_2$(acac)* **C2** and *Ir(L3)$_2$(acac)* **C3**, were synthetized by the interchange of chlorine atoms in *[Ir(C^N)$_2$(μ-Cl)]$_2$* by acetylacetone (acac) [17]:

These new complexes were characterized by different technics in order to obtain as much information as possible about the properties of the complexes. In addition to consider aspects as the influence of the acac ligand, or of metalation, on the properties of the complexes, the effect of loss of symmetry on the 2-phenylpyridine ligands, and the electronic effect of donors or acceptor substituents on it, has to be analyzed. As a whole, this information should help to predict if **C1**, **C2** or **C3** would be suitable for solar cells or OLED applications (see Schemes 3 and 4).

4.1.1. NMR experiments

C1: The complexation of the monoanionic ligand acetylacetonate in **5** is detectable by the appearance of two signals in the ^{1}H NMR spectrum due to the presence of acac (Fig. S1), corresponding to an allyl proton (5.2 ppm) and the methyl group of acac (2.20 ppm). Additional signals at 1.78 ppm and 4.0 ppm are assigned to the corresponding methyl protons and to the methyl ester groups present in the phenyl ring and pyridine ring, respectively. Table 1 shows the complete chemical shift assignment for the ^{1}H and ^{13}C spectra of **C1** obtained by means of the concerted

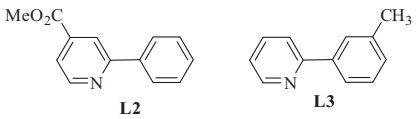

Scheme 2. Structure of 2-phenylpyridine ligands **L2** and **L3**.

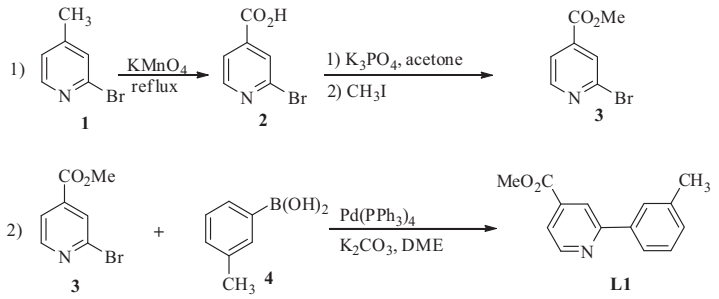

Scheme 1. Synthetic route to obtain 2-phenylpyridine, **L1**.

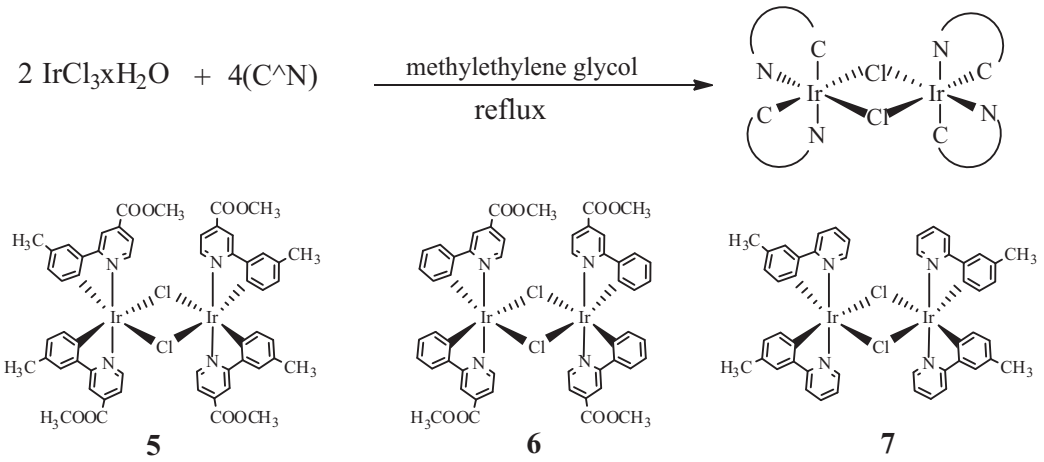

Scheme 3. Preparation of $[Ir(C^N)_2(\mu\text{-}Cl)]_2$; **5**, **6**, and **7**.

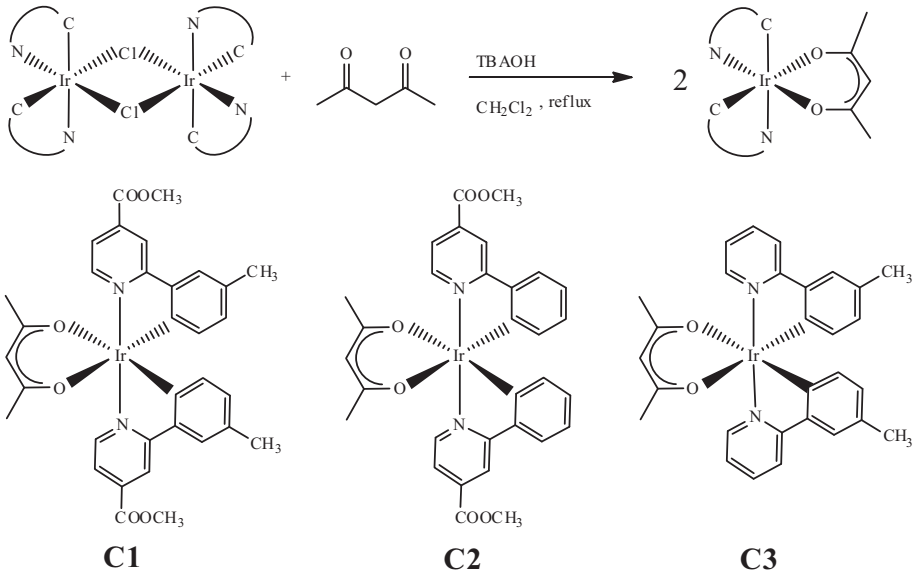

Scheme 4. Preparation of $[Ir(C^N)_2(acac)]_2$ type complexes; **C1**, **C2**, and **C3**.

application of a variety of one- and two-dimensional techniques: COSY, detecting one-bond (C–H), heteronuclear multiple quantum coherence (HMQC), and long-range two- and three-bond C–H heteronuclear multiple bond connectivity (HMBC).

2D ^{1}H homonuclear COSY spectrum (Fig. 1) showed the expected two-spin system as two doublets resonating at 7.63 and 8.63 ppm. The more deshielded doublet at 8.63 ppm corresponds to H_a (proton numbering given in the Figure of Table 1) and that at 7.63 corresponds to H_b,. The spectrum also showed other 2 two spin systems, attributed to the vicinal coupling between H_d and H_e. However so far it is not possible to indicate which is which.

The complete ^{1}H and ^{13}C NMR chemical shift assignments for **C1** was deduced from the concerted application of ^{1}H-detected "one-bond" and long-range (C,H) correlation experiments. The one-bond proton-carbon chemical shift correlation was established using the HMQC sequence (Fig. S2); all the "one-bond" (C,H) connectivities found between the pairs of mutually coupled atoms are given in Table 1.

The HMBC spectrum shows long-range correlations between Ha and three carbon resonances (Fig. S3). Examining the structure of **C1**, the resonance corresponding to C_2, and two quaternary carbons C_3 and C_5 can be identified. C_5 quaternary carbons show long range correlation with H_c and H_f, while C_6 correlates with H_c and H_d. Also, the quaternary C_7 corresponds to the signal resonating at 143.39 ppm which correlates at long-range with H_e and H_f. By examining the structure of **C1**, H_b correlates long-range with the quaternary carbons C_{12} and C_1. The resonance at 117.66 ppm is assigned to C_4, because it is long- range connected with H_b. The assignment of the other quaternary carbon resonance was straightforward. The quaternary carbon resonating at 184.77 ppm is assigned as C_{16}.

4.1.2. X-ray crystal structures

Crystal Structures for complexes $Ir(L1)_2(acac)$ (**C1**), $Ir(L2)_2(acac)$ (**C2**), and $Ir(L3)_2(acac)$ (**C3**) were determined. Displacement ellipsoids drawings of the compounds **C1**, **C2**, and **C3** are displayed in Figs. 2–4, respectively, and the crystal data and coordination geometrical parameters are listed in Tables 2 and 3. The crystallographic data for all the structures reported have been deposited in the Cambridge Database[1]. All the crystals were obtained from

[1] Crystallographic data (excluding structure factors) for the structures reported in this paper have been deposited in the Cambridge Crystallographic Data Centre as supplementary publication no. CCDC 997795–997797. Copies of the data can be obtained free of charge on application to CCDC, 12 Union Road, Cambridge CB2 1EZ, UK (fax: (044) 1223 336 033; e-mail: deposit@ccdc.cam.ac.uk).

Table 1
Assignment of ^{1}H and ^{13}C NMR of $[Ir(L1)_2(acac)]$ (**C1**).

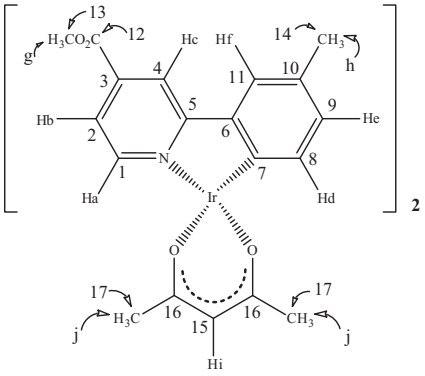

$^{1}H^{*}$	δ (ppm)	$^{13}C^{*}$	δ (ppm)	$^{13}C^{**}$	δ (ppm)
H_a	8,63	C_1	148,28	C_3	137,5
H_b	7,63	C_2	120,63	C_5	169,4
H_c	8,38	C4	117.66	C_6	143,14
H_d	6,1	C_8	132,41	C_7	143,39
H_e	6,57	C_9	130,95	C_{10}	129,99
H_f	7,48	C_{11}	125,12	C_{13}	52,75
H_g	4,04	C_{12}	165,01	C_{17}	28,55
H_h	2,2	C_{14}	20,85		
H_i	5,2	C_{15}	100,34		
H_j	1,78	C_{16}	184,77		

* Shows the direct bond between H-C.
** Quaternary carbon.

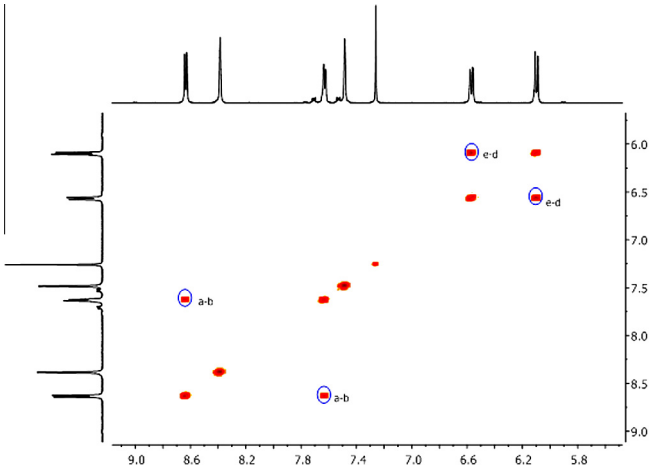

Fig. 1. COSY spectrum of **C1**.

mixed solution of dichloromethane and n-hexane. Complex **C1** crystallizes with one acetonitrile molecule which lies on a twofold axis. In the complexes **C2** and **C3**, the complete molecule is generated by crystallographic twofold symmetry, with the Ir and **C2** atoms lying on the rotation axis. For complexes **C1** and **C2**, the crystal structure is stabilized only by van der Waals interactions. However for complex **C3**, the crystal structure is stabilized by van der Waals interactions and by further stacking interaction between phenyl and pyridine moieties, in which the stacking distance is 3.6876 (17) Å and α = 3.70(14)° (α = dihedral angle between centroids defined by N11/C12-C16 and C21/C26 planes), Fig 5. As depicted in Figs. 2–4, the three complexes adopt distorted-octahedral coordination geometry with a *cis*-O,O, *cis*-C,C, and *trans*-*N,N* chelate disposition, and with angles of the *trans* ligands at the metal center range

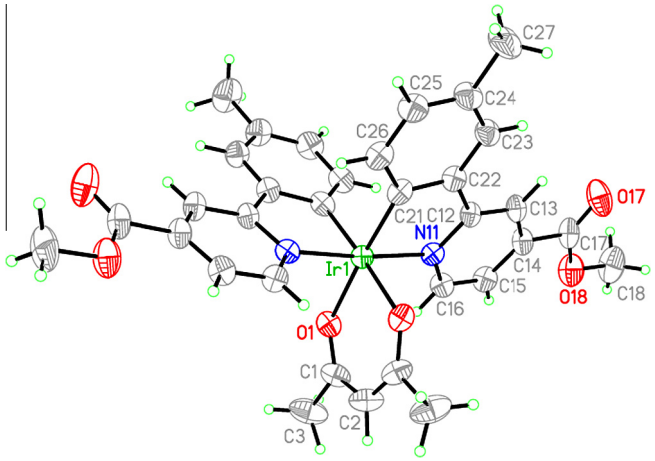

Fig. 2. Displacement ellipsoids drawing of **C1** showing the labeling scheme of atoms at 30% probability level. The acetonitrile solvent molecule was omitted for clarity.

between 175.31(15) and 176.7(2)°. The shortest coordination distances are associated with the Ir–C bonds while the longest are related to Ir–O bonds. The average Ir–O bond length observed in the complexes [2.147(4) Å] is considerably longer than the mean Ir–O value of 2.088 Å reported in the Cambridge Crystallographic Database and reflects the pronounced *trans* influence of the phenyl rings.

A comparison of the complexes indicates that complex **C2** possesses the shorter Ir–O distances [2.142(3) vs 2.149(4) Å] indicative of a comparatively weaker transophobic behavior [21].

In the three complexes, the C–Ir–C and N–Ir–N bond angles assume the order **C2** < **C3** < **C1**; **C3** < **C2** < **C1** respectively, while the O–Ir–O angles assume the order **C3** < **C1** < **C2**. Geometrical parameters such as bond lengths and angles around the Ir atom are in a similar range than reported for other $(C^{\wedge}N)_2Ir(acac)$ complexes [22–24].

In the complex **C1**, **C2** and **C3** the dihedral angles between pyridine and phenyl rings of the ppy ligands are 8.4(4)° and 5.5(4)°; 5.1(2)° and 3.7(14)° respectively. The relatively small dihedral angles between the aromatic rings are consistent with a large amount of conjugation across the ppy ligand. The electronic properties of the aromatic system are not affected by this effect [25].

4.2. Spectrophotometric study

UV–Vis absorption spectra for complexes **C1**, **C2** and **C3** measured in acetonitrile solution at room temperature are shown in Fig. 6, and the corresponding data in Table 4. The spectral data for the corresponding dimer precursors is shown in Table S4. As reported in literature [22] for compounds of type **C1**, **C2** and **C3**, strong bands with several maximum up to 300 nm appear and are attributed to intraligand (π–π^{*}) transitions. At lower-energy, absorption bands corresponding to metal-to-ligand charge transfer (MLCT) transitions are also present.

Regarding these last bands, it can be observed that in the case of **C3**, the presence of a donor methyl group in the **L3** ligand raises the energy of the LUMO orbital, enhancing therefore the HOMO–LUMO gap and explaining in this way the hypsochromic shift of the absorption pattern of this complex in regard to the other complexes of the series. Additionally, the presence of an electro withdrawing group in **L1** and **L2**, by stabilizing the LUMO orbital, also explains the tendency observed.

The emission spectrum of all complexes was registrated in acetonitrile solution, and is shown in the Supplementary Material. The

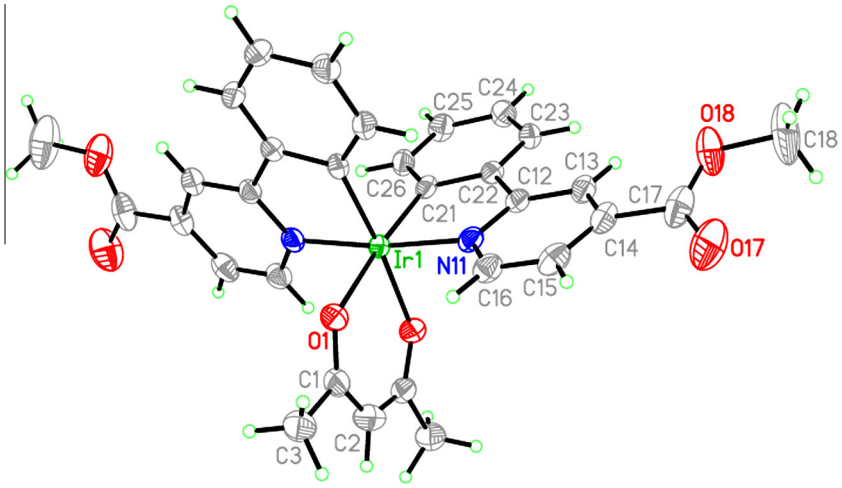

Fig. 3. Displacement ellipsoids drawing of **C2** showing the labeling scheme of atoms at 30% probability level.

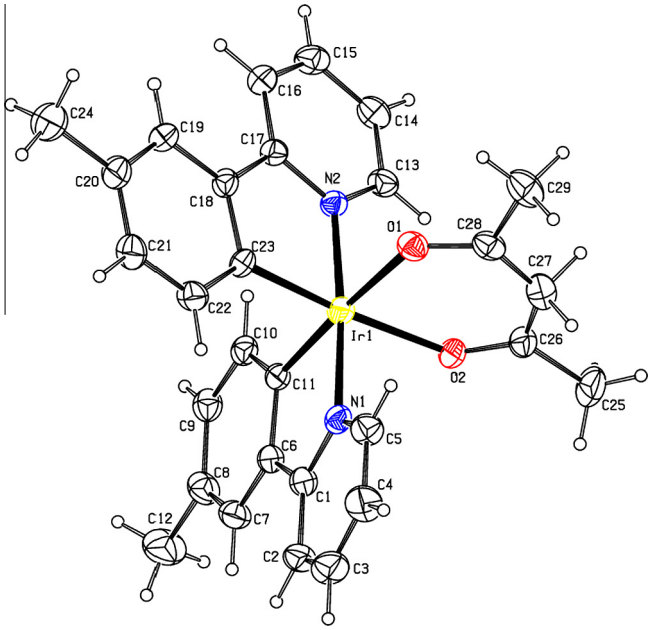

Fig. 4. Displacement ellipsoids drawing of **C3** showing the labeling scheme of atoms at 30% probability level.

presence of the electron withdrawing ester substituent in **C1** and **C2** generates dual emission and the expected displacement of the emission maxima to lower energy. Additionally, a close to one order of magnitude higher quantum yield is observed for **C3**, as can be seen in Table 5. In general, the three complexes studied in this work show a considerable weaker emission than the parent **C0** compound. This behavior is probably due to a combination of the shift to lower energies of the emission, generated specially by the presence of the esther substituent in **C1** and **C2**, and the introduction of substituents that increases the number of vibrational modes available for non-radiative deactivation. Indeed, **C3** is a better emitter than **C1** and **C2**. Although dual emission is not uncommon for Iridium(III)–polypyridine complexes in glass at low temperature, it is more rare in fluid solutions at room temperature, while some recent examples can be found in literature [26,27]. This behavior has been explained on the basis of an interruption of communication between the two emitting states, *e.g.* a triplet intraligand ^{3}IL and a triplet charge transfer ^{3}CT excited state [26].

4.3. Electrochemical studies

The complexes reported in this work possess different functional groups in their structure, in order to enable electronic transfer (ET) modulation. Despite that all complex show both the oxidation of the metal and the reduction of the ligand, the present study was mainly focused on the metal oxidation process.

In Fig. 7 the cyclic voltammetry of **C1**, **C2** and **C3** is displayed. For all complexes a *quasi*-reversible signal between 0.70 and 0.95 V was observed. These results correlate well with the structure of the complexes because the complex that is easier to oxidize ($E^{ox}_{1/2}$ = 0.733V) is **C3**, due to the presence of a methyl group that confers electron donating capacity to the ligand, facilitating the abstraction of one electron from the metal. On the other hand, in **C2** the presence of a withdrawing group generates a reduction of electronic density on the metallic center, increasing the energy needed to remove an electron. For **C1** the presence of both types of substituents balances the described behaviors, reflected in an oxidation potential between both values. Specifically, a difference of 116 mV between **C1** and **C3** and of 205 mV between **C2** and **C3** is observed, while a difference of 89 mV between **C1** and **C2** is observed, (see Table 6 and Fig. 7).

4.4. Theoretical calculations

4.4.1. Geometry optimization

In order to obtain the closest approximation to the real geometry of the molecules, obtained by X-ray crystallography, several exchange–correlation functional were tested on **C3**. The mean absolute deviation (MAD) was calculated and the xc correlation functional that minimizes these values, was chosen. In this sense, the OPBE functional appeared to be the best performing when employed in conjunction with a scalar relativistic correction. The values found are displayed in Table 6.

Comparing these values with those from crystallographic data of Table 3, a mean deviation of 0.019, 0.015 and 0.011 Å is found respect to the interatomic experimental distance, and a net difference of ±1° for bond angles was observed. When analyzing the above values, it can be seen that, as expected, the negative charge on the carbon atoms of the phenyl fragment enlarges the metal-acac oxygen atomic distance, *i.e.* the octahedral symmetry appears

Table 2
Crystal data for complexes **C1**, **C2** and **C3**.

Properties	Complex **C1**	Complex **C2**	Complex **C3**
Emprical formula	$2(C_{29}H_{28}Ir\ N_2O_2)\cdot(CH_3CN)$	$C_{33}H_{31}IrN_2O_6$	$C_{31}H_{27}IrN_2O_6$
Fw (Dalton)	669.82	743.80	715.74
T (K)	293(2)	173(2)	173(2)
Radiated used (λ(Å))	0.71073	0.71073	0.71073
Crystal size (mm^3)	0.30 × 0.26 × 0.24	0.320 × 0.280 × 0.130	0.140 × 0.110 × 0.020
Crystal system	monoclinic	orthorhombic	monoclinic
Space group	*C2/c*	*Pccn*	*C2/c*
a (Å)	26.144(5)	7.4478(5)	12.8967(6)
b (Å)	9.4460(19)	23.430(2)	13.7225(5)
c (Å)	22.784(5)	17.4357(15)	15.1286(7)
α (°)	90	90	90
β (°)	106.63(3)	90	92.677(4)
γ (°)	90	90	90
V ($Å^3$)	5391.2(19)	3042.6(4)	2674.5(2)
Z	4	4	4
ρ_{calc} ($g\ cm^{-3}$)	1.600	1.624	1.778
μ (mm^{-1})	4.983	4.435	5.041
F(000)	2560	1472	1408
Scan range θ (°)	1.63–26.14	2.870–25.007	2.514–25.341
Number of total reflections	10608	9121	15,171
Number of unique reflections (R_{int})	5245 (0.0280)	2668 (0.0426)	2455 (0.0691)
Number of data/restraints/parameters	5245/0/327	2668/0/194	2455/0/184
Goodness-of-fit (GOF) on F^2	1.080	0.969	1.087
R_1, wR_2 [$I>\sigma2(I)$]	0.0437 and 0.1224	0.0437 and 0.1168	0.0202 and 0.0482
R_1, wR_2 (all data)	0.0506 and 0.1225	$R1$ = 0.0466 and 0.1167	0.0214 and 0.0487

Table 3
Selected bond distances (Å) and bond angles for complexes **1**, **2** and **3**.

Complex	Ir–C (Å)	Ir–O (Å)	Ir–N (Å)	N–Ir–N(°)	C–Ir–C(°)	O–Ir–O(°)	C–Ir–N(°)	N–Ir–O(°)	C–Ir–O (°)
C1	1.993(6)	2.143(5)	2.049(5)	175.3(2)	94.2(2)	88.03(19)	80.5(2)	87.0(2)	88.0(2)
	2.003(6)	2.149(4)	2.054(5)				95.7(2)	96.5(2)	176.7(2)
							96.4(3)	96.9(2)	175.3(2)
							80.9(3)	86.4(2)	89.9(2)
C2	1.985(5)	2.142(3)	2.031(4)	174.3(2)	89.1(3)	88.45(18)	80.70(18)	94.61(14)	175.31(15)
							95.20(17)	89.49(14)	91.43(18)
C3	1.994(3)	2.155(2)	2.029(3)	172.54(13)	91.42(16)	87.80(12)	80.73(11)	91.16(9)	174.67(9)
						94.03(11)	94.21(9)	90.61(11)	

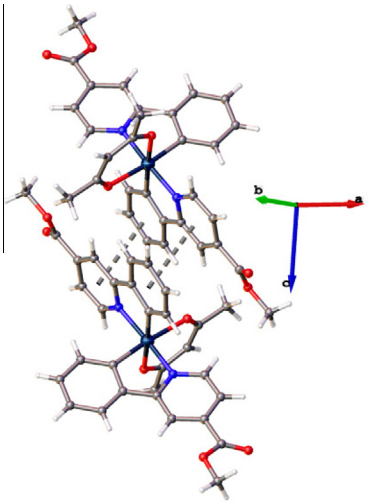

Fig. 5. A partial view of the crystal packing of the complex **3**, showing the weak π–π stacking interactions.

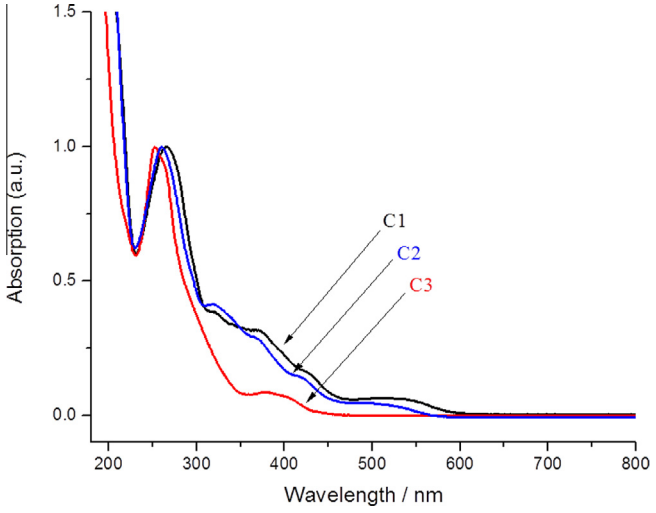

Fig. 6. Absorption bands of **C1**, **C2** and **C3** complexes in acetonitrile.

with a minor distortion, in a similar way than reported for analogous complexes [22].

4.4.2. Molecular orbital structure

Molecular orbital calculations were performed with scalar relativistic correction in presence of acetonitrile as solvent. Results displayed on Fig. 8 show the same orbital ordering tendency for the three complexes under study in regard to the unsubstituted Ir(ppy)$_2$(acac) complex, **C0**, used as reference. The differences between them can be understood in terms of Hirschfeld fragment analysis of the molecular orbitals for the four complexes. In this sense, the phenylpyridine ligand is decomposed in two

Table 4
Absorption maxima for complexes **C1**, **C2** and **C3** in acetonitrile.

Maximum absorption (nm)					
C1		**C2**		**C3**	
λ_1	265	λ_1	253	λ_1	261
λ_2	320	λ_2	262	λ_2	319
λ_3	374	λ_3	340	λ_3	369
λ_4	424	λ_4	380	λ_4	400
λ_5	531	λ_5	500		

Table 5
Emission maximums and emission quantum yields of **C1**, **C2** and **C3**.

$[Ir(ppy)_2](acac)$	**C0**[*]	**C1**	**C2**	**C3**
λ_{max} (nm)	516	622 657	597 611	520
ϕ_{emis}	0.34	2.24×10^{-3}	9.01×10^{-3}	1.40×10^{-2}

[*] Ref. [22], in 2-methyltetrahydrofuran solutions.

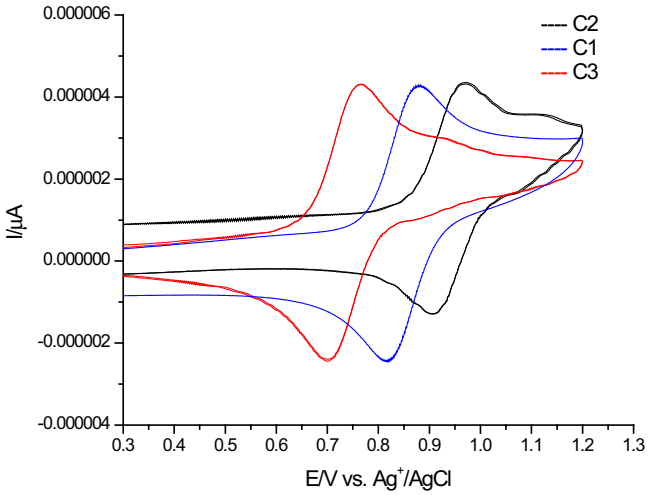

Fig. 7. Cyclic Voltammetry for **C1**, **C2** and **C3** in ACN, HFPBA 0.1 mol/L, scan rate of 100 mV/s.

Table 6
Calculated interatomic distances (Å) and bond angles.

Complex	Ir–C	Ir–O	Ir–N	N–Ir–N	C–Ir–C	O–Ir–O
C1	1.972	2.163	2.007	174	92	88
C2	1.967	2.171	2.003	174	91	85
C3	1.968	2.166	2.015	176	90	88

components: the phenyl (F) and pyridyl (P) fragments, while the other fragments are labeled as: (M) for the metal core and (L) for the ancillary ligand (acac). Additionally, the phenylpyridyne ligands are differentiated by labels 1 and 2. Results are depicted in Fig. 8(a).

Among these three complexes **C3** possesses the higher energy gap (2.42 eV). The methyl substituent on the cyclometallated ring causes a destabilization of the HOMO in 0.16 eV and 0.11 eV in the LUMO, with respect to the unsubstituted complex, **C0**. On the other hand, the electron withdrawing substituent ($-COOCH_3$), on complex **C2**, located on the pyridine ring, causes the stabilization of the HOMO (0.18 eV) and more markedly, of the LUMO (0.66 eV). The net result is the reduction of the band gap energy of this complex which is reflected in a bathochromic shift of the emission maxima (Table 5). The presence of a methyl group in the 4-position of the pyridine ring in **C1** is also reflected in the calculated results, particularly in a raise of 0.16 eV in the HOMO, with the consequent reduction of the band gap from 2.03 to 1.98 eV. Experimentally, this is observed by a further displacement of the emission to lower energy. These results are in agreement with similar substituent electronic effects reported by Baranoff [28].

Fig. 8(b) displays the composition of each molecular orbital in terms of the molecular fragments (P,F,M,L). As a general survey it can be mentioned that the HOMO is composed mostly by M (50%) and F (40%) components which result from a mixture of d + π^* atomic orbitals. The HOMO-1 also contains a combination of metal and ligand orbitals but in this case the ligand is acac (60%). At deeper energies the HOMO-2 is mainly metallic (76%) with small contribution of orbitals from all the ligands.

Looking the unoccupied molecular orbitals, it follows that the LUMO and LUMO + 1 are very close in energy, and mainly composed by the pyridyl (P1, P2) fragments of each ppy ligands. In a truly octahedral symmetry complete degeneration would be observed, but calculations and crystallographic data show that the octahedra are distorted, and that the two ppy ligands are asymmetric. This asymmetry is the cause of the lost of degeneracy of the LUMO, that is split in two sub-levels each one composed by only one ligand. The energy gap created between the LUMO and LUMO + 1 is of 30 meV for **C0**, and diminishes to 24 meV for **C3**, with the methyl substituted ppy ligand, while it increases to 40 and 45 meV when the methyl ester group is present like in **C1** and **C2**. At this point it is interesting to highlight that for all the complexes the HOMO, HOMO − 1,LUMO and LUMO + 1 contains the same fragment composition, however they differ in their% of participation. Nevertheless, at the LUMO + 2 a noticeable dissimilarity appears that differences **C0** and **C1** from **C2** and **C3**. In the case of the first two, this molecular orbital is centered on the ancillary (L) ligand while for the second pair it is centered on the ppy ligand.

4.5. Absorption and emission

Calculated TDDFT values for the complexes studied in presence of acetonitrile as solvent are displayed in Table 7. The forthcoming analysis starts with complex **C3**, which has a methyl substituent on para position on the phenyl fragment of the cyclometalated ligand. The absorption properties of the **C3** complex should be quite similar to those reported for the parent complex $(ppy)_2Ir(acac)$, **C0**. In general this type of complexes displays a strong absorption in the UV region (300–400 nm) and two less intense bands in the visible region, above 400 nm. For **C3** a low intensity band at 443 nm is found, with oscillator strength of 0.026. This band is composed by an HOMO-1 to LUMO electronic transition with two competing electron transfer reaction involved: a MLCT from the metal to the pyridine ring (M → P), and an electronic (L → P) transition from the *acac* ligand to the P fragment, which can be described as LLCT. Moving to lower energy values, an absorption can be found at 488 nm, with oscillator strength of $f = 0.009$, associated to the HOMO–LUMO transition and composed by two excitations: one with MLCT character and another Ligand Centered excitation (LC), originated on a charge transfer from the Phenyl (F) to the Pyridyl (P) fragment. The same assignment is proposed for the bands of complex **C0** .

When the electron withdrawing $COOCH_3$ group is introduced on the para position of the pyridine ring as in complex **C2**, a remarkably change in the absorption spectra is observed: a medium intensity band appears in the visible region at 403 nm with oscillator strength of 0.100 followed by a lower energy excitation at 536 nm with oscillator strength of $f = 0.052$ and displaying MLCT and LLCT character.

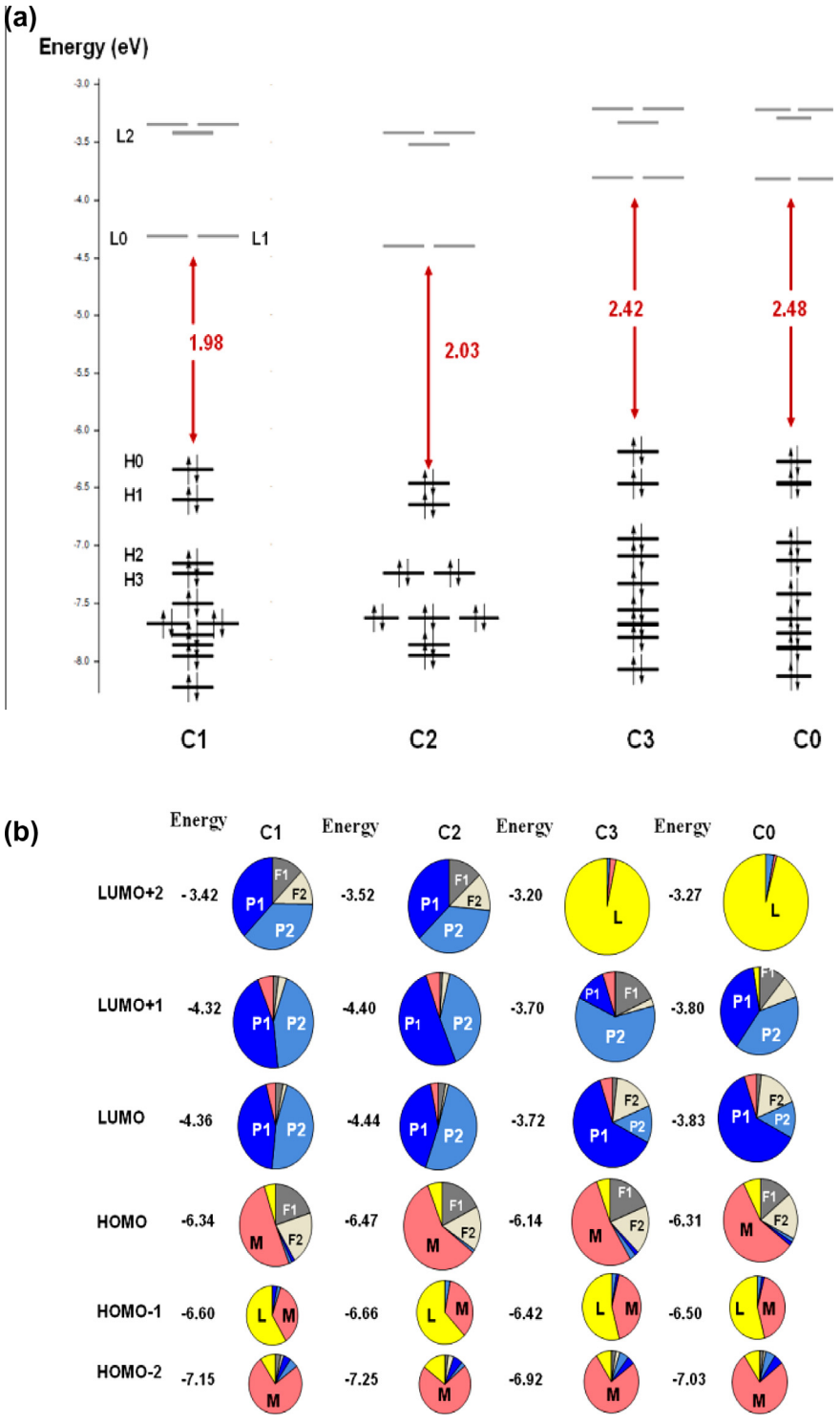

Fig. 8. (a) Molecular Orbital Diagram, (b) Composition of molecular orbital and its energies in term of fragment components (blue: phenyl (F), grey: pyridyl (P), pink: metal (M) and yellow: acac (L). Phenylpyridine ligands are differentiated by labels 1 and 2. (Color online.)

In principle the $COOCH_3$ group with its electron withdrawing character causes a stabilization of the LUMO from −3.72 eV to −4.44 eV which cause a bathochromic shift of the absorption band, originated on the HOMO-1 to LUMO transition, which for **C3** occurs at 443 nm and in **C2**, moves to 536 nm. The influence of the ester substituent is not only limited to a change in the energy at which this electronic transition occurs. It is also accompanied with an increase in the oscillator strength from 0.26 to 0.52.

Analyzing the **C1** complex, which is equivalent to **C2**, calculations reveals that this substituent do not alter significantly the position of the λ_{max} of both transition (403 and 532 nm). However, an increase on the oscillator strength of the higher energy transition is observed.

On the other hand, and looking to the composition of the HOMO and HOMO-1 for **C1**, **C2**, and **C3** it can be seen that the presence of a methyl ester group does not alter meaningfully the composition of

Table 7
Calculated values from TDDFT.

Compound	Electronic transition	λ (nm)	Oscillator strength	Main excitation	Nature	Description
C1	1a	532	0.051	88%H1 → L0	M + L → P	MLCT/^{3}LLCT
	1b	405	0.114	48%H0 → L2	M → P	MLCT
				28%H2 → L1	M + F → P + F	MLCT/^{3}LC
C2	2a	536	0.052	85%H1 → L0	M + L → P	MLCT/^{3}LLCT
	2b	403	0.100	57%H0 → L2	M + F → P	MLCT/^{3}LC
				57%H0 → L2	M + F → P	MLCT/^{3}LC
				22%H2 → L1	M → P	MLCT
C3	3a	443	0.026	90%H1 → L0	M + L → P	MLCT/^{3}LLCT

Table 8
Composition and calculated values for the two lowest triplets.

State	λ_{EM}[a] (nm)	Mono excitation	Description	Experimental
Complex **C1**				
T_1	622	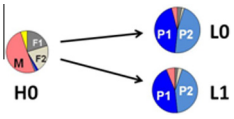	[c]MLCT/[c]LC	
T_2	637		[c]MLCT/[c]LC	622-657[b]
Complex **C2**				
T_1	609	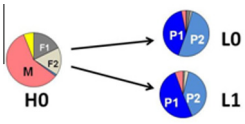	[c]MLCT/[c]LC	
T_2	622		[c]MLCT/[c]LC	597-611[b]
Complex **C3**				
T_1	516	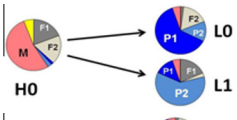	[c]MLCT/[c]LC/[c]LLCT	
T_2	521		[c]MLCT/[c]LC/[c]LLCT	520[b]
Complex **C0**				
T_1	503	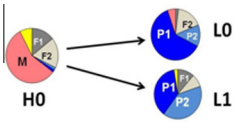	[c]MLCT/[c]LC/[c]LLCT	
T_2	508		[c]MLCT/[c]LC/[c]LLCT	516[c]

[a] Calculated.
[b] This work.
[c] Ref. [22].

these orbitals. This is not the case for the LUMO and LUMO + 1, where the composition of the molecular fragments is quite different for **C1** and **C0** respect to **C2** and **C3**, where for the later the Phenyl fragment does not contribute. Apparently the absence of this fragment could result in an increase of the oscillator strength on the transition involving these orbitals, allowing some electron transfer process which in the presence of the F2 fragment is forbidden.

Table 8 displays values for the two triplet non allowed lowest excitations, T1 and T2. Because of their energetic proximity and similar nature, these excitations need to be examined together; they involve HOMO–LUMO and HOMO–LUMO + 1 excitations, while the LUMO and LUMO + 1 are quasi degenerate levels. A third triplet can also be mentioned, but it occurs at higher energies and its role is not relevant for the present discussion. In general for the complexes under study two type of transitions are found: ^{3}MLCT and ^{3}LC. For the case of complexes with no substituent on the pyridyl ring (**C0**, **C3**), a third process is observed that correspond to a Ligand to Ligand Charge Transfer, arising between two similar fragments, but in different ligands. This new transition results from the increased participation of a Phenyl fragment (10–13%) in the LUMO and LUMO + 1 of the above mentioned complexes which is not found on the other complexes.

Regarding emission, considering in first place the unsubstituted complex **C0**, an emission arising from T1 and T2 is predicted at 503 and 508 nm, above the experimental value of 516 nm. **C3**, with a methyl substituent on the phenyl ring, shows a bathocromic shift on both triplets which is also observed on the experimental value. Moreover, the gap between the two triplets remains constant (5 nm) and is not influenced by this substituent. A different picture is found when an ester group is present on the pyridine ring (**C2**), which results in a bathocromic shift of the calculated emission mean value, $(\lambda_{EM}(T1)+ \lambda_{EM}(T2))/2$, from 518 nm to 616 nm. Another point to mention is the increase of gap between the two triplets (13 nm) giving rise to a broadening of the emission band. Interestingly, adding a methyl group to the phenyl ring as in complex **C1**, results in new red shift displacement of the calculated emission mean value to 630 nm. The larger bathocromic shift occurring from 506 nm in **C0** to 630 nm on **C1** can be understood in terms of the collaborative effect occurring between the electron withdrawing substituent on the pyridine ring, which stabilizes the LUMO, and the electron donating substituent on the phenyl ring which destabilize the HOMO. This theoretical considerations correlate well with the experimental emission spectra (Fig. S16, Suplementary Material) in the sense that **C2** shows a broadening of the emission band, while in **C1**, where the gap between T1 and T2 is enhanced, dual emission is clearly observed.

It can be mentioned that a preliminar analysis of the applicability of the compounds in devices was tested. In this line, IPCE analysis was performed for [Ir(L1)$_2$(acac)], **C1**, and [Ir(L2)$_2$(acac)], **C2**, due that both complexes have an ester group to act as an anchor to TiO_2 when incorporated in a photoelectrochemical Grätzel type solar cell prototype. **C1** showed a higher efficiency than **C2**, while both complexes have quite low yield efficiency compared to **N3** (cis-Bis(isothiocyanato) bis(2,2'-bipyridyl-4,4'-dicarboxylato ruthenium(II)) and [Ir(dtp)(tpy-COOH)]PF_6, an Iridum complex

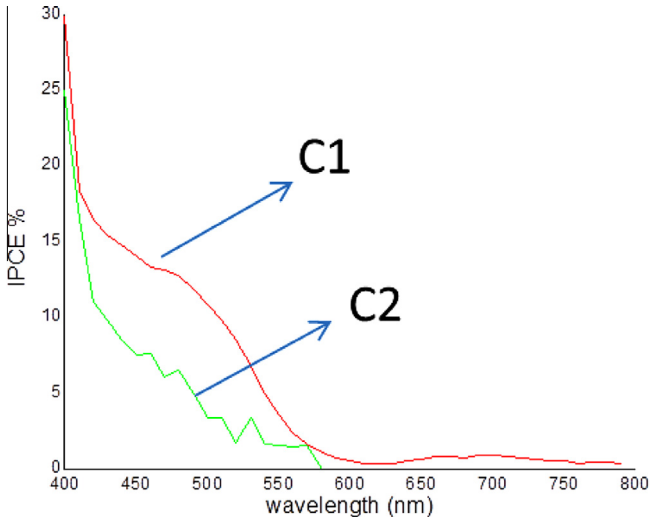

Fig. 9. Action spectra for complexes **C1** and **C2**.

with an efficiency of 63% [29], under the same experimental conditions. Fig. 9 shows the action spectra for complexes **C1** and **C2**.

The difference observed between **C1** and **C2** can be explained by the enhanced panchromaticity of **C1** in the red part of the visible region of the spectra. The injection capacity of **C1** could also be enhanced because of the presence of an electronic donating substituent as CH_3 that induces an increment of charge density available to be injected [30]. It has been postulated in literature that a raise in the degree of asymmetry – in this case due to different substituent groups on the phenyl and pyridine rings can cause an increase in the value of the molar extinction coefficient ε.

Regarding the potentiality of these complexes in emitting devices, can be seen in Table 7, compound **C3** is the best emitter of the series. This is not surprising, in the sense that according to Fig. 8 this compound shows a greater energy gap than **C1** and **C2**, that diminishes the non radiative decay paths, according to the energy gap law. Nevertheless, Evans [31] establishes some requirements to be fulfilled by complexes of this type to be efficient in OLED devices. Among the variables analyzed are the emission wavelength, lifetime and phosphorescence quantum yield. Considering the quantum yield, the requirement in this case is that it should have a value of at least 0.25 at 298 K [32]. As **C3** displays a quantum yield of 0.014, according to this criteria, its expected performance in an OLED device would be low [33].

One of the possible causes of the predicted low response could be the reduced aromaticity of the ligand structure. Additionally, the donor effect of the methyl group seems not to be preponderant in the modification of the HOMO and LUMO, showing little effect.

5. Conclusions

Non-symmetric substituted phenylpyridine (ppy) type ligands were designed and synthesized. The effect of the presence of a methyl donor group on the phenyl group of ppy and of a carboxylate acceptor group on the pyridine moiety was evaluated, and tested on the corresponding $[Ir(C^N)_2(acac)]_2$ type complexes. The complexes were characterized by different NMR techniques and X-ray crystal structure determination. In the three complexes the geometrical parameters such as bond lengths and angles around the Ir atom are in a similar range than reported for other $[Ir(C^N)_2(acac)]_2$) complexes.

In general, higher similarities among the physicochemical properties of compounds **C1** and **C2** than between **C1** and **C3** are observed. In this sense, the withdrawing electronic effect of the ester group seems to predominate. By theoretical and electrochemical studies it was established that for **C3**, the methyl electron donor group destabilizes the HOMO and LUMO levels, generating a an energy gap of 2.17 eV, greater than for **C1** and **C2**, causing evidently two spectroscopic consequences, the first is a bathochromic shift of the emission maxima, and the second concerns the dual emission band produced by S1 and Triplet close levels (1.72–1.78 eV) allowing to observe a joined fluorescence and phosphorescence bands. Finally, it can be mentioned that, for the reasons given above, although not behaving in the range of the expected values for a good response, **C3** would be the best compound to be tested in light emitting devices, while the di-substituted compound **C1** would be the best to be tested as dye in a solar cell.

Acknowledgements

This work was supported by the project Fondecyt 1110991 and the Project "Puente VRI" of the Pontificia Universidad Católica de Chile.

Appendix A. Supplementary data

CCDC contains the supplementary crystallographic data for 997795–997797. These data can be obtained free of charge via http://www.ccdc.cam.ac.uk/conts/retrieving.html, or from the Cambridge Crystallographic Data Centre, 12 Union Road, Cambridge CB2 1EZ, UK; fax: (+44) 1223-336-033; or e-mail: deposit@ccdc.cam.ac.uk. Supplementary data associated with this article can be found, in the online version, at http://dx.doi.org/10.1016/j.poly.2016.07.029.

References

[1] J. Caspar, T.J. Meyer, Inorg. Chem. 22 (17) (1983) 2444.
[2] (a) M. Grätzel, Inorg. Chem. 44 (20) (2005) 6841;
(b) G.J. Meyer, Inorg. Chem. 44 (2005) 6852;
(c) S. Ardo, G.J. Meyer, Chem. Soc. Rev. 38 (2009) 115;
(d) A.M. Bunzli, E.C. Constable, C.E. Housecroft, A. Prescimone, J.A. Zampese, G. Longo, L. Gil-Escrig, A. Pertegás, E. Ortí, H.J. Bolink, Chem. Sci. 6 (2015) 2843;
(e) P. Dreyse, B. Loeb, M. Soto-Arriaza, D. Tordera, E. Ortí, J.J. Serrano-Pérez, H.J. Bolink, Dalton Trans. 42 (2013) 15502;
(f) S. Fantacci, F. De Angelis, S. Fantacci, F.A. De Angelis, Coord. Chem. Rev. 255 (2011) 2704.
[3] Ch. Liu, X. Rao, X. Lv, J. Qiu, Z. Jin, Dyes Pigm. 109 (2014) 13.
[4] (a) M. Sykora, M.A. Petruska, J. Alstrum-Acevedo, I. Bezel, T.J. Meyer, V.I. Klimov, J. Am. Chem. Soc. 128 (2006) 9984;
(b) A. Beeby, S. Bettington, I.D.W. Samuel, Z. Wang, J. Mater. Chem. 13 (2003) 80;
(c) B. Aranda, P. Aguirre, S.A. Moya, M. Bonneau, J.A.G. Williams, L. Toupet, M. Escadeillas, H. Le Bozec, V. Guerchais, Polyhedron 86 (2015) 120.
[5] J. Frey, B.F.E. Curchod, R. Scopelliti, I. Tavernelli, U. Rothlisberger, M.K. Nazeeruddin, E. Barano, Dalton Trans. 43 (2014) 5667.
[6] T. Sajoto, P.I. Djurovich, A. Tamayo, M. Yousufuddin, R. Bau, M.E. Thompson, R.J. Holmes, S.R. Forrest, Inorg. Chem. 44 (2005) 7992.
[7] R. Wang, D. Liu, H. Ren, T. Zhang, X. Wang, J. Li, J. Mater. Chem. 21 (2011) 15494.
[8] (a) P.J. Hay, J. Phys. Chem. A 106 (8) (2002) 1634;
(b) C. Liu, X. Rao, X. Lv, J. Qiu, Z. Jin, Dalton Trans. 41 (2012) 2582;
(c) I. González, D. Cortés-Arriagada, P. Dreyse, L. Sanhueza-Vega, I. Ledoux-Rak, D. Andrade, I. Brito, A. Toro-Labbé, M. Soto-Arriaza, S. Caramori, B. Loeb, Eur. J. Inorg. Chem. (2015) 4946.
[9] A.J. Hallett, N. White, W. Wu, X. Cui, P.N. Horton, Simon J. Coles, Jianzhang Zhaob and S.J.A. Pope, Chem. Commun. 48 (2012) 10838.
[10] G. Velde, F.M. Bickelhaupt, S.J.A. Van Gisbergen, C. Fonseca Guerra, E.J. Baerends, J.G. Snijders, T. Ziegler, J. Comput. Chem. 22 (2001) 931.
[11] (a) N.C. Handy, A.J. Cohen, Mol. Phys. 99 (2001) 403;
(b) J.P. Perdew, K. Burke, M. Ernzerhof, Phys. Rev. Lett. 77 (1996) 3865;
(c) M. Swart, A.W. Ehlers, K. Lammertsma, Mol. Phys. 103 (2004) 2467.
[12] Smith, P. Burn, B. Powell, ChemPhysChem 12 (2011) 2429.
[13] F.L. Hirshfeld, Theor. Chim. Acta 44 (1977) 129.
[14] Klamt, G. Schüürmann, Perkin Trans. 2 (1993) 799.
[15] O. Gritsenko, P. Schipper, E. Baerends, Chem. Phys. Lett. 302 (1999) 199.

[16] H. Hashizume, H. Ito, N. Kanaya, H. Nagashima, H. Usui, R. Oshima, M. Kanao, H. Tomoda, T. Sunazuka, T. Nagamitsu, H. Kumagai, S. Omura, Heterocycles 38 (1994) 1551.
[17] S. Sprouse, K.A. King, P.J. Spellane, R.J. Watts, J. Am. Chem. Soc. 106 (1984) 6647.
[18] C.-H. Yang, J. Beltran, V. Lemaur, J. Cornil, D. Hartmann, W. Sarfert, R. Frohlicj, C. Bizzarri, L. De Cola, Inorg. Chem. 49 (2010) 9891.
[19] E. Baranoff, S. Suarez, P. Bugnon, H.J. Bolink, C. Klein, R. Copelliti, L. Zuppiroli, M. Grätzel, M.K. Nazeeruddin, ChemSusChem 2 (2009) 305.
[20] E. Baranoff, J.H. Yum, I. Jung, R. Vulcano, M. Grätzel, M.K. Nazeeruddin, Chem. Asian J. 5 (2010) 496.
[21] J. Vicente, A. Arcas, D. Bautista, M.C.R. de Arellano, J. Organomet. Chem. 663 (2002) 164.
[22] S. Lamansky, P. Djurovich, D. Murphy, F. Abdel-Razzaq, R. Kwong, I. Tsyba, M. Bortz, B. Mui, R. Bau, M.E. Thompson, Inorg. Chem. 40 (2001) 1704.
[23] R.M. Edkins, A. Wriglesworth, K. Fucke, S.L. Bettington, A. Beeby, Dalton Trans. 40 (2011) 9672.
[24] E. Baranoff, B.F.E. Curchod, J. Frey, R. Scopelliti, F. Kessler, I. Tavernelli, U. Rothlisberger, M. Grätzel, M.K. Nazeeruddin, Inorg. Chem. 51 (2012) 215.
[25] J.L. Brédas, G.B. Street, B. Thémans, J.M. André, J. Chem. Phys. 83 (1985) 1323.
[26] K.Y. Zhang, H.-W. Liu, M.-C. Tang, A. Wing-Tat Choi, N. Zhu, X.-G. Wei, K.-C. Lau, K. Kam-Wing Lo, Inorg. Chem. 54 (2015) 6582.
[27] S. Kumar, Y. Hisamatsu, Y. Tamaki, O. Ishitani, and S. Aoki, 2016, DOI: http://dx.doi.org/10.1021/acs.inorgchem.5b02872.
[28] F. Kessler, R.D. Costa, D. Di Censo, R. Scopelliti, E. Ortiz, H.J. Bolink, S. Meier, W. Sarfert, M. Grätzel, M.K. Nazeeruddin, E. Baranoff, Dalton Trans. 41 (2012) 180.
[29] Y. Shinpuku, F. Inui, M. Nakai, Y. Nakabayashi, J. Photochem. Photobiol., A 222 (2011) 203.
[30] (a) G. Volpi, C. Garino, L. Salassa, J. Fiedler, K.I. Hardcastle, R. Gobetto, C. Nervi, Chem. Eur. J. 15 (2009) 6415;
(b) F. Geist, A. Jackel, R.F. Winter, Dalton Trans. 44 (2015) 3974;
(c) D.N. Kozhevnikov, V.N. Kozhevnikov, M.Z. Shafikov, A.M. Prokhorov, D.W. Bruce, W.J.A. Gareth, Inorg. Chem. 50 (2011) 3804.
[31] R.C. Evans, P. Douglas, C. Winscom, J. Coord. Chem. Rev. 250 (2006) 2093.
[32] (a) E.M. Kober, J.V. Caspar, R.S. Lumpkin, T.J. Meyer, J. Phys. Chem. 90 (1986) 3722.
[33] P. Liehm, C. Murawski, M. Furno, B. Lüssem, K. Leo, M.C. Gather, Appl. Phys. Lett. 101 (2012) 253304.